PAPER

Check for updates

High surface area 3D-MgO flowers as the modifier for the working electrode for efficient detection of 4-chlorophenol†

Khursheed Ahmad[a] and Shaikh M. Mobin *[abc]

We report for the first time, magnesium oxide (MgO) 3D-flowers, synthesized by a simple reflux method. The synthesized MgO 3D-flowers were characterized by powder X-ray diffraction (PXRD), ultra-violet visible (UV-vis) spectroscopy, scanning electron microscopy (SEM) and energy-dispersive X-ray (EDX) mapping to confirm their purity, morphology and elemental composition. The synthesized MgO 3D-flowers had a very high specific surface area of 218 m^2 g^{-1} as confirmed by the N_2 adsorption–desorption isotherm. These MgO 3D-flowers were employed as an electrode modifier for the construction of an electrochemical sensor to detect 4-chlorophenol (4-CP). The active surface area of the glassy carbon electrode (GCE) was modified with MgO 3D-flowers with the assistance of 0.1% Nafion (MgO 3D-flowers/GCE) and the MgO 3D-flowers/GCE sensor shows an excellent electrocatalytic behavior towards 4-CP. The constructed MgO 3D-flowers/GCE sensor exhibits the limits of detection (LOD) of 45 nM, 68 nM, and 52 nM, and sensitivities of 2.84 μA μM^{-1} cm^{-2}, 5.94 μA μM^{-1} cm^{-2}, and 10.67 μA μM^{-1} cm^{-2} in cyclic voltammetry (CV), differential pulse voltammetry (DPV) and square wave voltammetry (SWV) techniques, respectively. The modified MgO 3D-flowers/GCE sensor displays excellent performance in terms of sensitivity, selectivity, repeatability and reproducibility. The excellent electrocatalytic activity of the proposed MgO 3D-flowers/GCE sensor was attributed to the high specific surface area, surface electron transfer ability and the presence of the edges/corner defects of MgO 3D-flowers.

1. Introduction

Recently, inorganic self-assembled nanostructured materials have attracted researchers' attention.[1] The physiochemical properties of nanomaterials could be controlled by their morphologies and architecture.[2–4] Specifically, three dimensional (3D) nanostructures have gained much attention because of their application in various fields such as water treatment, pigments, sensors, cosmetics, energy and catalysis. Various methods such as solvothermal, template-assisted growth and hydrothermal have been developed to synthesize 3D-nanostructured materials.[1]

In particular, magnesium oxide (MgO) is a wide band gap semiconductor which has been employed in various applications such as photoluminescence, adsorption,[5] field emission,

templates, catalysis,[6–8] photo-catalysis, electrochemical sensors, waste water treatment, electronics and photovoltaic applications.[1,5–8] Since, the properties of MgO nanostructures strongly depend on the synthetic method, various efforts have been made to synthesize MgO by employing different methods such as solvothermal, electrochemical, precipitation, chemical vapour deposition, carbothermic reduction, electro-spinning, template, sol–gel, pyrolysis, epitaxial growth and microwave and sonochemical.[9] The commonly obtained morphologies of MgO include nanosheets/nanoplates/nanoflakes, nanorods, lamella-like, tubular tetrapods, columnar structures, rectangular parallelepipeds, spheres, rectangular sheets, fibers/whiskers, cubes, flower-like and nanobelts.[10–20] Every method or technique has its own advantages/disadvantages, but it still remains a challenge to develop new architectures or a simple protocol to synthesize MgO with improved properties such as a high surface area. We have synthesized MgO by using the reflux method, and the obtained results showed the flower-like structure of MgO with an improved surface area which is more desirable for catalytic reactions.

Phenolic compounds containing one or more aromatic rings, especially 4-chloro-phenol (4-CP), are widely used in various industrial applications (insecticides, herbicides, fungicides, dyes and disinfectants).[21] 4-CP has been considered

[a]Discipline of Chemistry, Indian Institute of Technology Indore, Simrol, Khandwa Road, Indore 453552, India. E-mail: xray@iiti.ac.in; Tel: +91 731 2438 752

[b]Discipline for Biosciences and Bio-Medical Engineering, Indian Institute of Technology Indore, Simrol, Khandwa Road, Indore 453552, India

[c]Discipline of Metallurgy Engineering and Material Science, Indian Institute of Technology Indore, Simrol, Khandwa Road, Indore 453552, India

† Electronic supplementary information (ESI) available. See DOI: 10.1039/c8na00007g

a highly toxic pollutant which has hazardous effects on the environment as well as human beings.[21] Due to the potent toxicity of 4-CP, rapid and sensitive detection of 4-CP is of great importance to save human health and the environment. Various techniques have been employed for the determination of 4-CP; among them gas chromatography (GC) and high performance liquid chromatography (HPLC) are widely used methods but they suffer from bulky instruments and cumbersome sample preparation.[22,23] Therefore, in the search of an alternative method for the sensing of pollutants, the electrochemical method has been considered the most effective and promising technique due to its low cost and ability to detect the analyte with high sensitivity and selectivity along with fast response.[24] In the last few years, various nanomaterials (ZnO, NiO, CO_3O_4, SnO_2, MnO_2, CuO, TiO_2, $SrTiO_3$ etc.)[25–30] with different structures have been investigated to fabricate an electrochemical sensor.

Recently, our research group investigated different electrocatalysts (MnO_2, TiO_2 and $rGO/SrTiO_3$) for the construction of electrochemical sensors.[28–30] In continuation, we have now studied the electrochemical behavior of MgO 3D-flowers and constructed an electrochemical sensor to detect 4-CP.

2.   Materials and methods

2.1.   Chemicals and reagents

Sodium carbonate (Na_2CO_3), magnesium chloride hexahydrate ($MgCl_2 \cdot 6H_2O$) and phosphate buffered saline solutions were purchased from Molychem, India. Nafion was purchased from Sigma Aldrich and was used as received. All the other chemicals were purchased from Merck and Alfa Aesar which were used as received.

2.2.   Instrumental

The powder X-ray diffraction patterns (PXRD) were recorded on a RINT 2500 V X-ray diffractometer (Rigaku, Japan) with Cu Kα radiation ($\lambda = 1.5406$ Å). The morphology and elemental constituents of the samples were characterized by using a Supra 55 Zeiss Field Emission Scanning Electron Microscope (FESEM) coupled with energy dispersive X-ray (EDX) spectroscopy (Oxford Instruments' X-max, Aztec). Spectrophotometric measurements were performed on a Varian UV-vis spectrophotometer (model: Carry 100). The specific surface area and textural parameters were obtained by using the Brunauer–Emmett–Teller (BET) method with an Autosorb iQ, version 1.11 (Quantachrome Instruments). All electrochemical measurements were performed on a computer-controlled Metrohm Autolab PGSTAT 204N using a GCE as a working electrode, a platinum wire as a counter electrode and Ag/AgCl as a reference electrode with NOVA software, version 1.10.

2.3   Synthesis of magnesium oxide (MgO) 3D flowers

20 mL of a 1 M sodium carbonate (Na_2CO_3) solution (H_2O) was added to 20 mL of a 1 M magnesium chloride hexahydrate ($MgCl_2 \cdot 6H_2O$) solution (polyethylene glycol = PEG) slowly and was stirred at 90 °C for 2 h. The white precipitate was collected

by centrifugation and washed with D.I. water several times and calcined at 550 °C for 2 h.

2.4   Preparation of a MgO 3D-flower-modified glassy carbon electrode (MgO 3D-flowers/GCE)

A glassy carbon electrode (GCE) with a diameter of 3 mm was polished with an alumina slurry and sonicated for 20 minutes to remove any residual impurity. 10 μl of MgO 3D-flowers (5 mg 10 mL^{-1}) with 0.1% Nafion dissolved in D.I. water was drop cast onto the active area of the GCE electrode, and the electrode was kept under ambient conditions to dry for 3 h.
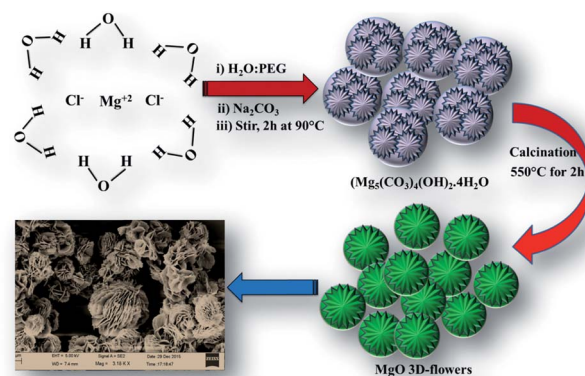
3.   Results and discussion

3.1   Synthesis of MgO

A facile reaction between aqueous Na_2CO_3 and $MgCl_2 \cdot 6H_2O$ dissolved in PEG for 2 h at 90 °C under continuous stirring followed by calcination at 550 °C yielded MgO 3D flowers (Scheme 1).[18,19]

3.2.   Characterization

The PXRD analysis was performed to check the phase purity and crystallinity of the synthesized MgO 3D-flowers. The XRD pattern of the MgO 3D-flowers exhibited well-defined diffraction peaks which are consistent with previously reported literature (JCPDS no. 01-1235). The diffraction peaks appearing at 36.67°, 42.75°, 61.97°, 74.56° and 78.44° were attributed to the (111), (200), (220), (311) and (222) planes, respectively (Fig. 1). The average crystallite size of the MgO 3D-flowers was calculated to be 97.4 nm by using Debye–Scherrer's equation.

Furthermore, no additional diffraction peak was observed for any impurity ions, which confirms the high phase purity of the MgO 3D-flowers. The morphological characteristics of the prepared MgO 3D-flowers were investigated using FE-SEM analysis. Fig. 2 shows the FE-SEM images of the MgO 3D-flowers at different magnifications. From the recorded images, it was observed that the synthesized MgO 3D-flowers exhibited a flower-like structure with a smooth surface.

Scheme 1   Schematic representation of the synthesis of MgO 3D-flowers.
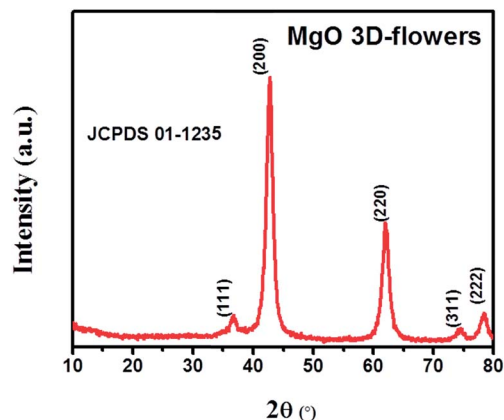
Fig. 1 XRD pattern of the MgO 3D-flowers.

Furthermore, to confirm the phase purity and elemental composition of MgO 3D-flowers, EDX analysis was carried out. The obtained results confirm the high phase purity and presence of Mg and O elements (Mg = 28.27 wt% and O = 71.87 wt%) as shown in Fig. 3A. The elemental mapping shows the presence of Mg and O with no impurities which confirmed the formation of MgO 3D-flowers (Fig. 3B and C). The UV-vis absorption spectrum of the MgO 3D-flowers is presented in Fig. 3D. Absorption bands in the range of 2.5–5.0 eV generally appear due to spatial defects of O_{LC} present in MgO.[30,31] The obtained UV-vis spectrum for MgO 3D-flowers shows two bands at 231 nm and 317 nm which are assigned to the O_{LC}^{2-} ion present in MgO 3D-flowers at the edges (O_{4C}^{2-}) and corner sites (O_{3C}^{2-}), respectively.[31,32]

The N_2 adsorption/desorption analysis was performed to probe the surface area and porosity of MgO 3D-flowers, and the N_2 isotherm is presented in Fig. 3E. The obtained result shows that the MgO 3D-flowers have a high specific surface area of 218 m^2 g^{-1}, which is larger than those of the previously reported MgO nanostructures (Table S1†).

It is well known that nanomaterials with unique morphological features and a high surface area are more favorable to achieve high performance for electrochemical applications. Furthermore, these MgO 3D-flowers were used as an electrode modifier to construct an electrochemical sensor for the detection of 4-CP.

3.3 Optimized conditions for MgO 3D-flower formation

To optimize the time for the formation of MgO 3D-flowers, we have performed FE-SEM (Fig. S1†) at different time periods which shows that at initial stages (5–15 min), the MgO precursor accumulates as a small bunch and from 30 to 90 min, it starts growing into a bulky flower-like structure which was completely transformed into flower-like structures after 120 min. The PXRD analysis of this precursor matched with the composition of hydromagnesite ($Mg_5(CO_3)_4(OH)_2 \cdot 4H_2O$; JCPDS card no. 25-0513), and the results are shown in Fig. S2.† This hydromagnesite was further converted into MgO 3D-flowers on calcination at 550 °C for 3 h (Fig. 2).

3.4 EIS analysis of MgO 3D-flowers

Electrochemical impedance spectroscopy (EIS) is the most reliable and important tool to validate or investigate the electrocatalytic behavior of materials/electrocatalysts.[33–35] We have employed the EIS analysis to investigate the charge transfer kinetics and capacitive components of the MgO 3D-flowers. Fig. 4 shows the obtained Nyquist plots for the bare GCE and MgO 3D-flowers/GCE sensor in the presence of 5 mM redox probe [Fe(CN)6]$^{3-/4-}$, and the equivalent circuit is presented in the inset (Fig. 4). A well-defined semi-circle appeared for the GCE with a high charge resistance whereas a small semi-circle was obtained for the MgO 3D-flowers/GCE sensor which shows a lower charge resistance as compare to the GCE. It is well understood that a high charge resistance limits the electron transfer rate. The lower charge resistance of the MgO 3D-flowers/GCE sensor was attributed to the surface modification of the GCE with MgO 3D-flowers. The charge resistance for the bare GCE and MgO 3D-flowers/GCE sensor is summarized in
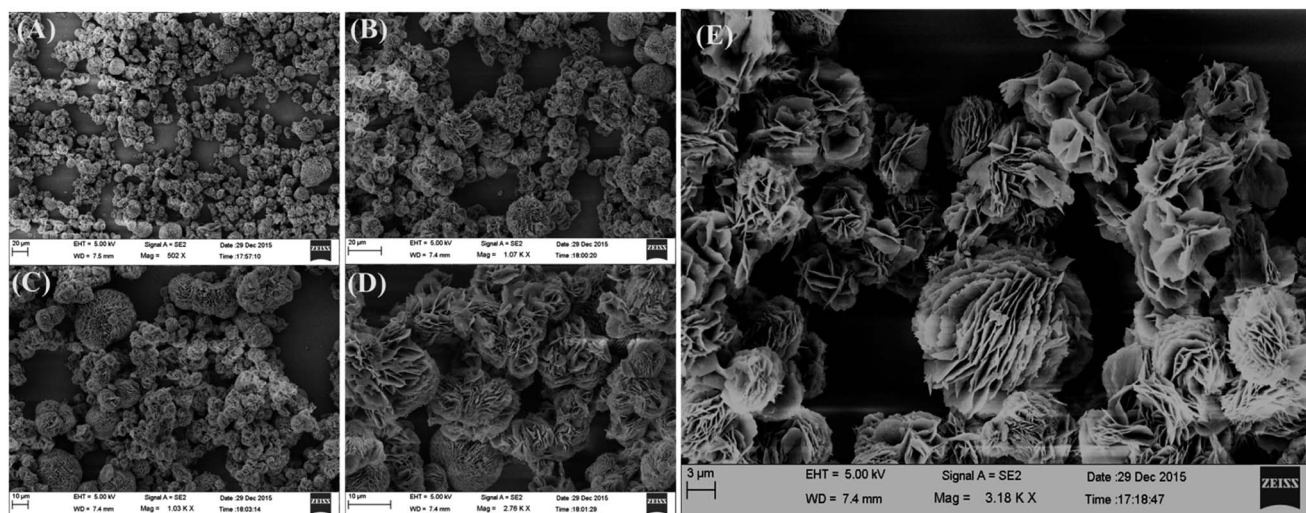

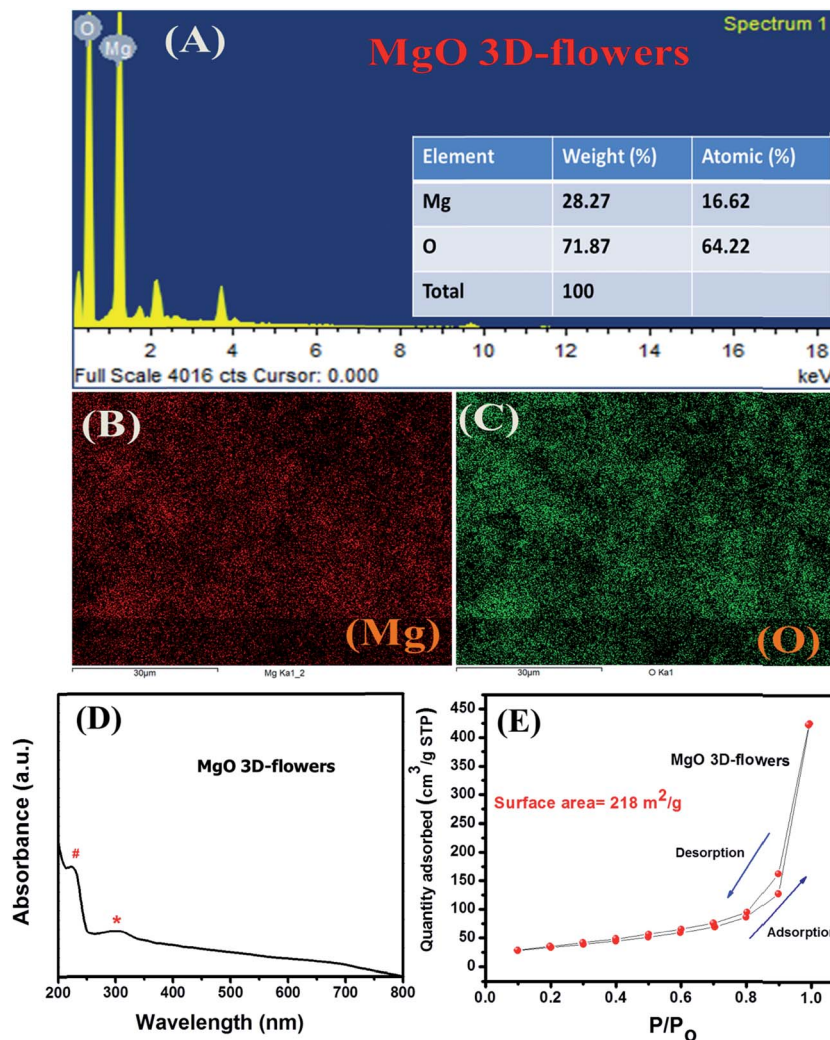Fig. 2 FE-SEM images of the MgO 3D-flowers at different magnifications (A–E).

Fig. 3 EDX spectrum (A), elemental mapping (B and C), UV-vis spectrum (D) and N_2 adsorption–desorption isotherm (E) of MgO 3D-flowers.

Table S2.† Furthermore, cyclic voltammetry for the bare GCE and MgO 3D-flowers/GCE sensor in the presence of 5 mM redox probe $[Fe(CN)6]^{3-/4-}$ was performed. Fig. 4B shows the cyclic voltammograms of the bare GCE and MgO 3D-flowers/GCE sensor, and a higher current was obtained for the MgO 3D-flowers/GCE sensor compared to the bare GCE which revealed the high electrocatalytic behavior of the MgO 3D-flowers/GCE

sensor. The obtained results are consistent with the EIS data and suggest that the electron transfer rate increases for the MgO 3D-flowers/GCE sensor which results in a higher current response due to the high electrocatalytic behavior of MgO 3D-flowers, which comes from their high surface area and several defects present in MgO 3D-flowers.[32]

3.5 Electrochemical study of the MgO/GCE sensor

The electrochemical oxidation behavior towards 4-CP was investigated for the bare GCE and modified MgO 3D-flowers/GCE sensor using four electrochemical techniques (cyclic voltammetry; CV, differential pulse voltammetry; DPV, square wave voltammetry; SWV and linear sweep voltammetry; LSV) in the presence of 25 μM 4-CP in 0.1 M phosphate buffered saline (PBS) solution at pH 7.0. Fig. 5A shows the CVs of the bare GCE and MgO 3D-flowers/GCE sensor in the presence of 25 μM 4-CP in 0.1 M PBS (pH 7.0) at a scan rate of 100 mV s^{-1}. A very sharp oxidation peak was observed for the bare GCE which can be due to the oxidation of 4-CP whereas the same trend was found for the MgO 3D-flowers/GCE sensor with an enhanced current response without any reduction peak which suggests that the
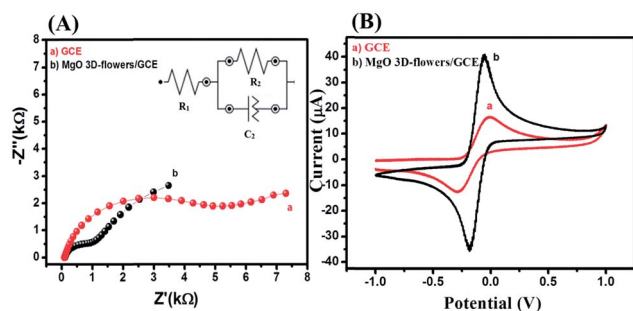

Fig. 4 Nyquist plots (A) and CVs (B) of the bare GCE (a) and MgO 3D-flowers/GCE sensor (b) in the presence of 5 mM K_3 [Fe(CN)$_6$]/ K_4[Fe(CN)$_6$] in 0.1 M PBS (pH = 7.0). Inset: equivalent circuit.
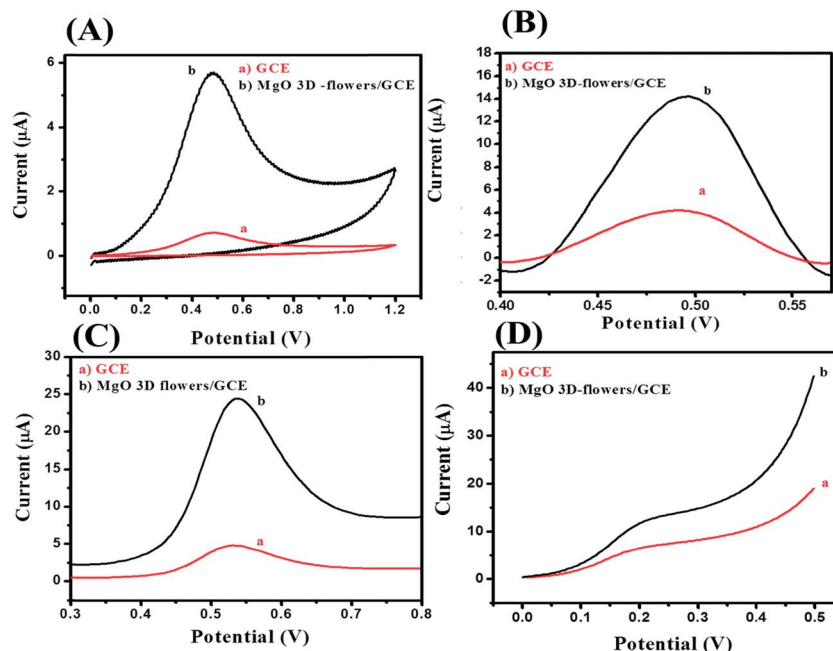
Fig. 5 Cyclic voltammograms (A), differential pulse voltammograms (B), square wave voltammograms (C) and linear sweep voltammograms (D) of the bare GCE and MgO 3D-flowers/GCE sensor in the presence of 25 μM 4-CP in 0.1 M PBS (pH 7.0) with a scan potential of 100 mV s^{-1}.

oxidation of 4-CP is an irreversible process. DPV which is a derivative of staircase voltammetry is considered a highly sensitive electrochemical technique to investigate reversible/ irreversible redox reactions/processes. We have recorded the DPVs of the bare GCE and MgO 3D-flowers/GCE sensor under similar conditions, and the MgO 3D-flowers/GCE sensor shows an enhanced current compared to the bare GCE with a single oxidation peak which further confirms that the oxidation of 4-CP is an irreversible process (Fig. 5B). Furthermore, SWV and LSV techniques were also employed to investigate the electro-catalytic behavior of the MgO 3D-flowers/GCE sensor towards the detection of 4-CP. Fig. 5C and D show the SWVs and LSVs of the bare GCE and MgO 3D-flowers/GCE sensor in the presence of 25 μM 4-CP, and a higher electrocatalytic current response with a sharp irreversible oxidation peak of 4-CP was observed for the MgO 3D-flowers/GCE sensor as compared to the bare GCE. Hence, it was concluded that the excellent electrocatalytic behavior of MgO 3D-flowers towards the oxidation of 4-CP in 0.1 M PBS at pH 7.0 has been proved using four different electrochemical techniques (CV, DPV, SWV and LSV).

This excellent electrocatalytic property of the MgO 3D-flowers was attributed to the presence of defects in MgO 3D-flowers and high surface area and low charge resistance. The performance of any sensor depends on various factors; among them, pH of the solution is most vital; therefore, we have investigated the effect of pH on the performance of the MgO 3D-flowers/GCE (Fig. 6). The observed studies revealed that with an increase in the pH value, the oxidation peak of the 4-CP shift towards a less positive potential value with a very high current response. The highest current was obtained at pH 7.0, and therefore, further studies on the electro-catalytic oxidation of 4-CP were carried out at pH 7.0.

The effect of the concentration (5–50 μM) of 4-CP on the modified MgO 3D-flowers/GCE in 0.1 M PBS at pH 7.0 with a 100 mV s^{-1} scan rate was checked by employing CV, DPV, and SWV techniques (Fig. 7A, C and D).

The electro-catalytic oxidation current response increased with increasing the concentration of the 4-CP, and the linear calibration curves (for CVs and SWVs) corresponding to the current *versus* concentration were plotted and are shown in Fig. 7B and E. The effect of scan rate on the performance of the MgO 3D-flowers/ GCE sensor towards 25 μM 4-CP was checked using cyclic voltammetry (Fig. 7F), and the electrocatalytic oxidation current increases with increments in the scan rate from 100 mV s^{-1} to 1000 mV s^{-1}. The linear calibration curve of the peak current *versus* square root of the scan rate has been presented in Fig. 7G.
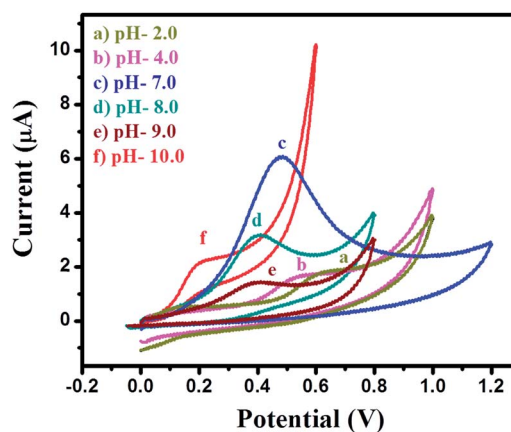

Fig. 6 Cyclic voltammograms of the MgO 3D-flowers/GCE sensor in the presence of 25 μM 4-CP in 0.1 M PBS at different pH (2, 4, 7, 8, 9 and 10) with a scan potential of 100 mV s^{-1}.
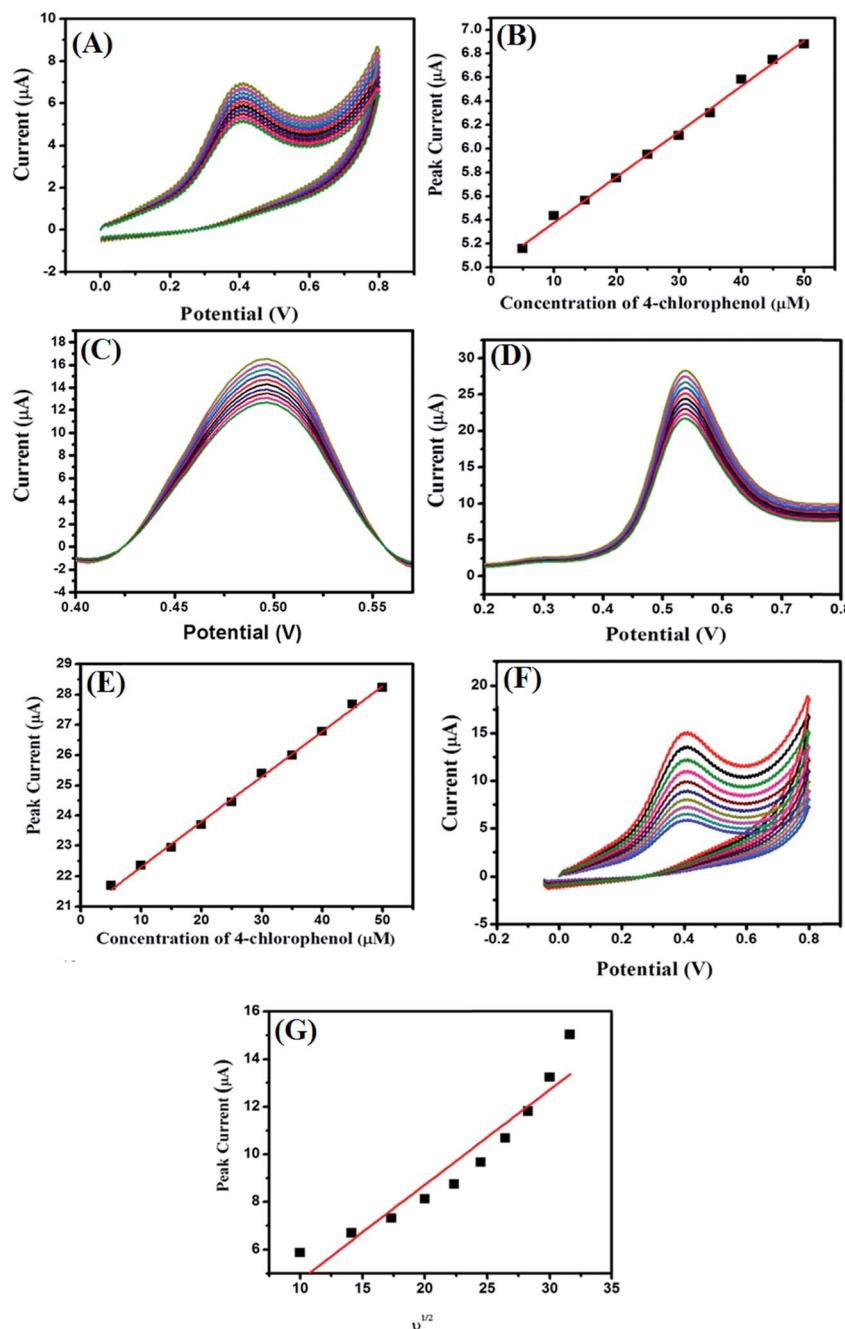
Fig. 7 CVs (A), DPVs (C), and SWVs (D) of the MgO 3D-flowers/GCE sensor in the presence of different concentrations of 4-CP (5–50 μM) in 0.1 M PBS (pH 7.0) with a scan rate of 100 mV s^{-1} and calibration plot of the corresponding peak current *versus* concentration for CVs (B) and SWVs (E); CVs of the MgO 3D-flowers/GCE sensor at different scan rates (100–1000 mV s^{-1}) in the presence of 25 μM 4-CP in 0.1 M PBS (pH 7.0) (F) and calibration plot of the peak current *versus* square root of the scan rate (G).

3.6 Proposed mechanism

During the electrochemical analysis, one oxidation peak was observed for the oxidation of 4-CP which was found to be irreversible.
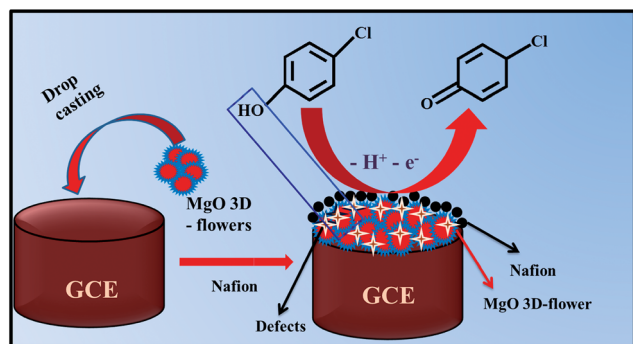
This oxidation process may be related to the interaction between the MgO 3D-flowers and analyte. This interaction may be due to the intermolecular effects between the O atoms in the lattice or the oxo-surface groups and the hydroxyl ions present in the 4-CP.[30,31] The probable mechanism for the oxidation of

4-CP involves the release of one electron which resulted in the formation of 4-chlorophenone (Scheme 2).

3.7 Interference study in the presence of different electro-active species

For practical applications, a sensor should possess an anti-interference behavior. Therefore, the interference study in the presence of different electroactive species (b–q) was performed for the MgO 3D-flowers/GCE sensor using the SWV method.

Scheme 2 Schematic representation of the surface modification of the GCE and proposed working mechanism for the detection of 4-CP.

Fig. 8 shows the DPVs of the MgO 3D-flowers/GCE sensor in the presence of various interference species such as Mg^{2+}, Pb^{2+}, Hg^{2+}, Na^+, K^+, lactose, citric acid, sucrose, glucose, toluene, nitro-toluene, aniline, nitro-aniline, nitrobenzene, catechol, nitro-phenol, benzaldehyde and chlorobenzene at a 10–50 times higher concentration than the 4-CP but no significant change in the overpotential and current response was observed. This revealed the high selectivity of the MgO 3D-flowers/GCE sensor towards the detection of 4-CP.

3.8 Reproducibility, repeatability and stability studies

The reproducibility of the MgO 3D-flowers/GCE sensor was evaluated by employing cyclic voltammetry for 6 freshly prepared modified electrodes (MgO 3D-flowers/GCE) in the presence of 25 μM 4-CP in PBS (pH 7.0) with a scan rate of 100 mV s^{-1}. The relative standard deviation (RSD) was calculated to be 2.41% for 6

electrodes which indicated the higher reproducibility of the MgO 3D-flowers/GCE sensor. The repeatability of the MgO 3D-flowers/GCE sensor was checked by recording 8 consecutive cycles of CV under the same conditions. The RSD was calculated to be 3.17% which confirms the good repeatable nature of the MgO 3D-flowers/GCE sensor. The MgO 3D-flowers/GCE sensor was stored for 10 days in a desiccator, and the current response was intermittently tested to check the stability of the sensor. The obtained current response after 10 days was found to be almost the same as that observed for the fresh electrode (Fig. S2†), and 96.7% of the initial current response was retained. The results showed that the MgO 3D-flowers/GCE sensor possesses good stability.

3.9 Comparison with the reported sensors

The electrochemical detection of 4-CP is of great significance due to its toxic nature and hazardous effects; several efforts have been made by surface modification of a GCE with different polymers, metal oxides, and hybrid materials such as horseradish peroxidase immobilized on partially reduced graphene oxide (HRP/PCRG), multi-wall carbon nanotubes/nano-nickel hydroxide (MWCNTs–Ni(OH)$_2$), gold/graphitic carbon nitride, polyvinyl alcohol (PVA)/Lac/PEO–PPO–PEO (F108)/gold nanoparticles (Au NPs) (PVA/F108/Au NPs/Lac), molecularly imprinted polymers and PDDA-functionalized graphene (PDDA-G/MIP), horseradish peroxidase-modified nanostructured Au thin films (HRP/Au), copper oxide, graphite–epoxy composite electrodes, multilayer graphene oxide/platinum and gold nanoparticles/carbon nanotubes. Most of the reported sensors involve polymers, expensive metal electrodes (Au, Pd *etc.*) or hybrid materials which limit their practical commercialization. It is still a great challenge to
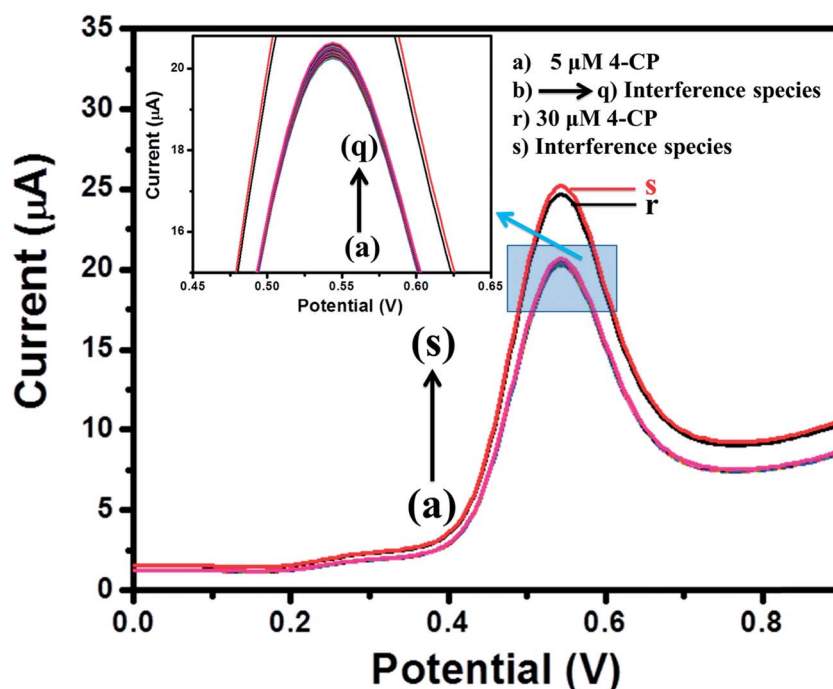

Fig. 8 Square wave voltammograms of the MgO 3D-flowers/GCE sensor in the presence of different interfering species.

Table 1 Comparison of the LOD, sensitivity and linear range for 4-CP with previously reported literature

No.	Electrode	Limit of detection (LOD) (nM)	Sensitivity	Linear range (μM)	Ref.
1	HRP/PCRG/GC	15 000	—	1–800	36
2	MWCNTs–Ni(OH)$_2$/GCE	500	—	1–750	37
3	Au/g-C$_3$N$_4$	80	—	—	38
4	PVA/F108/AuNPs/Lac GCE	12 000	—	1–25	39
5	PDDA-G/MIP/GCE	300	—	0.8–100	40
6	HRP/Au/GCE	390	3.96 μA/mM cm^2	2.5–47.5	41
7	SPCE/CuO	430	1.02 μA/μM cm^2	0.25–1	42
8	Graphite–epoxy composite electrode	10 000	0.042 mA mM^{-1}	100–500	43
9	MLG/Pt	54	1.21 μA/μM cm^2	0.5–10	24
10	AuNPs@cMWCNT–GCE	110	—	0.3–400	44
11	**MgO 3D-flowers/GCE (cyclic voltammetry)**	**45**	**2.84 μA/μM cm^2**	**10–45**	**This Work**
	MgO 3D-flowers/GCE (differential pulse voltammetry)	**68**	**5.94 μA/μM cm^2**	**5–50**	
	MgO 3D-flowers/GCE (square wave voltammetry)	**52**	**10.67 μA/μM cm^2**	**10–50**	

develop a highly selective, sensitive, low cost and stable sensor for the detection of 4-CP. We have developed for the first time, a highly selective and sensitive 4-CP sensor using MgO 3D-flowers as the electrocatalyst. This MgO 3D-flowers/GCE sensor shows an excellent limit of detection and sensitivity over the reported sensors listed in Table 1.

4. Conclusion

MgO flowers were synthesized by a simple reflux method. The synthesized MgO 3D-flowers were used as the electrode modifier for the construction of an electrochemical sensor for the detection of 4-chlorophenol. We have shown stepwise growth of MgO 3D-flowers by time-dependent FE-SEM studies which confirm formation of MgO 3D-flowers in 2 h. The MgO 3D-flowers/GCE sensor exhibits a decent limit of detection (LOD) and high selectivity towards 4-CP without any interference from other electro-active species in DPV and CA techniques. This MgO 3D-flowers/GCE sensor is reusable, highly stable and sensitive which makes it a potential candidate for practical applications.

Conflicts of interest

There are no conflicts to declare.

Acknowledgements

References

1 N. Sutradhar, A. Sinhamahapatra, S. K. Pahari, P. Pal, H. C. Bajaj, I. Mukhopadhyay and A. B. Panda, *ACS Appl. Mater. Interfaces*, 2016, **8**, 18173–18181.

2 C. Burda, X. Chen, R. Narayanan and M. A. El-Sayed, *Chem. Rev.*, 2005, **105**, 1025–1102.

3 H. R. Moon, J. J. Urban and D. J. Milliron, *Angew. Chem., Int. Ed.*, 2009, **48**, 6278–6281.

4 C. Yan, L. Nikolova, A. Dadvand, C. Harnagea, A. Sarkissian, D. F. Perepichka, D. Xue and F. Rosei, *Adv. Mater.*, 2010, **22**, 1741–1750.

5 C. Gao, W. Zhang, H. Li, L. Lang and Z. Xu, *Cryst. Growth Des.*, 2008, **8**, 3785–3790.

6 M. Verziu, B. Cojocaru, J. Hu, R. Richards, C. Ciuculescu, P. I. Filip and V. I. Parvulescu, *Green Chem.*, 2008, **10**, 373–381.

7 B. M. Choudary, M. L. Kantam, K. V. S. Ranganath, K. Mahendar and B. Sreedhar, *J. Am. Chem. Soc.*, 2004, **126**, 3396–3397.

8 S.-W. Bain, Z. Ma, Z.-M. Cui, L.-S. Zhang, F. Niu and W. G. Song, *J. Phys. Chem. C*, 2008, **112**, 11340–11344.

9 M. Sharma and P. Jeevanandam, *J. Alloys Compd.*, 2011, **509**, 7881–7885.

10 C. Yan, C. Sun, Y. Shi and D. Xue, *J. Cryst. Growth*, 2008, **310**, 1708–1712.

11 P. Jeevanandam, R. S. Mulukutla, Z. Yang, H. Kwen and K. J. Klabunde, *Chem. Mater.*, 2007, **19**, 5395–5403.

12 D. Chen, L. Zhu, P. Liu, H. Zhang, K. Xu and M. Chen, *J. Porous Mater.*, 2009, **16**, 13–18.

13 L. Qin, J. Zhao and X. Zou, *Mater. Chem. Phys.*, 2009, **113**, 468–473.

14 K. H. Kim, M. S. Lee, J. S. Choi and J. P. Ahn, *Thin Solid Films*, 2009, **517**, 3995–3998.

15 G. Wang, L. Zhang, H. Dai, J. Deng, C. Liu, H. He and C. T. Au, *Inorg. Chem.*, 2008, **47**, 4015–4022.

16 Z. Zhang, Y. Zheng, J. Chen, Q. Zhang, Y. Ni and X. Liang, *Adv. Funct. Mater.*, 2007, **17**, 2447–2454.

17 T. Selvamani, T. Yagyu, S. Kawasaki and I. Mukhopadhyay, *Catal. Commun.*, 2010, **11**, 537–541.

18 S.-W. Bian, J. Baltrusaitis, P. Galhotra and V. H. Grassian, *J. Mater. Chem.*, 2010, **20**, 8705–8710.

19 K. Mageshwari, S. S. Mali, R. Sathyamoorthy and P. S. Patil, *Powder Technol.*, 2013, **249**, 456–462.

20 Z. Zhou, Q. Sun, Z. Hu and Y. Deng, *J. Phys. Chem. B*, 2006, **110**, 13387–13392.

21 S. Sharma, M. Mukhopadhyay and Z. V. P. Murthy, *Ind. Eng. Chem. Res.*, 2010, **49**, 3094–3098.

22 K.-D. Wang, P.-S. Chen and S.-D. Huang, *Anal. Bioanal. Chem.*, 2013, **406**, 2123–2131.

23 R. Alizadeh, *Talanta*, 2016, **146**, 831–838.

24 P. K. Kannan, R. V. Gelamo, H. Morgan, P. Suresh and C. S. Rout, *RSC Adv.*, 2016, **6**, 105920–105929.

25 A. Maikap, K. Mukherjee, B. Mondal and N. Mandal, *RSC Adv.*, 2016, **6**, 64611–64616.

26 J. Saravanan, R. Ramasamy, H. A. Therese, G. Amala and G. G. kumar, *RSC Adv.*, 2015, **5**, 76538–76547.

27 Y. Zhou, X. Ni, Z. Ren, J. Ma, J. Xu and X. Chen, *RSC Adv.*, 2017, **7**, 45177–45184.

28 K. Ahmad, A. Mohammad and S. M. Mobin, *Electrochim. Acta*, 2017, **252**, 549–557.

29 K. Ahmad, A. Mohammad, R. Rajak and S. M. Mobin, *Mater. Res. Express*, 2016, **3**, 074005.

30 K. Ahmad, A. Mohammad, P. Mathur and S. M. Mobin, *Electrochim. Acta*, 2016, **215**, 435–446.

31 H. Li, M. Li, G. Qiu, C. Li, C. Qu and B. Yang, *J. Alloys Compd.*, 2015, **632**, 639–644.

32 H. Li, M. Li, W. Guo, X. Wang, C. Ge and B. Yang, *Electrochim. Acta*, 2014, **123**, 103–110.

33 N. Sutradhar, A. Sinhamahapatra, S. K. Pahari, P. Pal, H. C. Bajaj, I. Mukhopadhyay and A. B. Panda, *J. Phys. Chem. C*, 2011, **115**, 12308–12316.

34 L. Ai, H. Yue and J. Jiang, *Nanoscale*, 2012, **4**, 5401–5408.

35 A. Hanif, S. Dasgupta and A. Nanoti, *Ind. Eng. Chem. Res.*, 2016, **55**, 8070–8078.

36 Y. Zhang, J. Zhang, H. Wu, S. Guo and J. Zhang, *J. Electroanal. Chem.*, 2012, **681**, 49–55.

37 J. Zolgharnein, T. Shariatmanesh and A. Babaei, *Sens. Actuators, B*, 2013, **186**, 536–544.

38 L. Xu, S. Ling, H. Li, P. Yan, J. Xia, J. Qiu, K. Wang, H. Li and S. Yuan, *Sens. Actuators, B*, 2017, **240**, 308–314.

39 J. Liu, J. Niu, L. Yin and F. Jiang, *Analyst*, 2011, **136**, 4802–4808.

40 B. Wang, O. K. Okoth, K. Yan and J. Zhang, *Sens. Actuators, B*, 2016, **236**, 294–303.

41 C. Qiua, T. Chen, X. Wang, W. Li and H. Ma, *Colloids Surf., B*, 2013, **103**, 129–135.

42 F. Pino, C. C. Mayorga-Martinez and A. Merkoçi, *Electrochem. Commun.*, 2016, **71**, 33–37.

43 A. Bebeselea, F. Manea, G. Burtica, L. Nagy and G. Nagy, *Talanta*, 2010, **80**, 1068–1072.

44 L. Wang, Q. Sun, Y. Liu and Z. Lu, *RSC Adv.*, 2016, **6**, 34692–34698.